

Nonlinear dynamics of unicycles in leader-follower formation

Siming Zhao, Abhishek Halder, Tamás Kalmár-Nagy*

February 13, 2009

Abstract

In this paper, dynamical analysis is presented for a group of unicycles in leader-follower formation. The equilibrium formations were characterized along with the local stability analysis. It was demonstrated that with the variation in control gain, the collective dynamics might undergo Andronov-Hopf and Fold-Hopf bifurcations. An increase in the number of unicycles increase the vigor of quasi-periodicity in the regime of Andronov-Hopf Bifurcation and heteroclinic bursts between quasi-periodic and chaotic behavior in the regime of Fold-Hopf bifurcation. Numerical simulations also suggest the occurrence of global bifurcation involving the destruction of heteroclinic orbit.

1 Introduction

Equilibrium formations for nonholonomic systems have been an active area of research in recent times among many disciplines like biological sciences [1, 2, 3], computer graphics [4] and systems engineering [5, 6, 7, 8]. One particular problem studied in this context has been the *consensus seeking* [9] or the *state agreement problem* [10] which deals with designing feedback controllers to make multiple agents converge to a common configuration in the global coordinates. A special case to this is the *rendezvous problem* [11, 12] where the agents converge at a single location.

In addition to the stability and control aspects, considerable efforts have also been put in effective modeling of the nonholonomic systems to make the analysis tractable. Starting from the *n*-bug problem in mathematics [13], the self-propelled planar particles were later [14, 15] replaced by wheeled mobile agents with single nonholonomic constraint i.e. unicycles. Lie group formulation [16] and oscillator models [17] have been attempted for dynamic modeling of such agents. In particular, Klein and Morgansen [18] extended the oscillator model to account for the intermediate centroid velocity of the unicycles to make trajectory tracking possible.

Several researchers ([14], [15], [19], [20], [21]) proposed laws for designing control strategies of such nonholonomic vehicles. One possible approach to design the control law is to use a centralized cooperative control scheme for the

*S. M. Zhao, A. Halder and T. Kalmár-Nagy are with the Department of Aerospace Engineering, Texas A&M University, College Station, Texas, 77843, USA. {s0z0239, a0h7710, kalmarnagy}@aeromail.tamu.edu

entire agent collective. However, such a control law is susceptible to bandwidth limitation as well as external disturbances and hence not scalable for a team having large number of mobile agents. As a result, distributed control laws have been investigated by the researchers for this problem, where the feedback is constructed through local interactions of the vehicles leading to a global formation convergence. In particular, Yang et al. ([22], [23]) proposed a decentralized framework where a distributed controller accounts for local control decision based on the interaction of each agent with its neighbors. Moreover, their algorithm was also capable of estimating the global statistics of the swarm (for example, overall swarm shape), thereby enabling simultaneous estimation and control. A special research topic has been to design the distributed controller with asynchronous communication constraints. For a detailed account on this topic, the reader may refer [24], [25], [26] and [27].

The present paper is part of a research endeavor which aims to address the nonholonomic multi-agent dynamics and distributed control problem. The authors earlier studied [28] the cyclic pursuit of 2-unicycle problem with a controller similar to [14] in modified form. These preliminary results showed that the system may exhibit very different dynamics depending on the choice of controller gains and such regimes were calculated. As a next step, in this paper, the authors present nonlinear dynamics of multiple nonholonomic unicycles in leader-follower configuration to characterize similar regimes and system parameter dependence which, the authors believe, throws light in many non-trivial areas of the complex dynamics of the agents leading to greater understanding of the overall system. In this paper, the local stability analysis has been performed and numerical results are presented to illustrate the dynamics of the agent collective.

As outlined in the brief literature review, the differences in the recent research directions in multi-agent systems has generally varied with the variety of control strategies and the types of consensus demanded. To the best of the authors knowledge, very few attempts (like [29]) have been made to characterize the local stability of the system from the standpoint of nonlinear dynamics. While this is probably owing to the highly complex dynamics of the system, the authors must underline the fact that a successful analysis to even slightly simpler systems like leader-follower configuration, can guide us in better designing of controllers.

As mentioned above, choice of leader-follower configuration was partly due to its slightly simpler dynamics and partly due to the fact that many biological systems (like birds) also exhibit this configuration. This choice, in the biological world was long believed to be for energy efficiency [30]. Some recent results [31] tell that leader-follower configuration may also enhance communication and orientation of the flock. It is a topic of research whether this form may have any superiority in inter-agent communication and performance for the bio-mimetic collectives.

The rest of this paper is organized as follows. Section II describes the mathematical model considered in this paper and transforms the equations of motion from global coordinates to relative coordinates. Section III provides the derivation of fixed points followed by corresponding equilibrium formations. Section IV presents the stability boundary based on local stability analysis and associated Hurwitz stability criteria. Section V presents the existence of Andronov-Hopf bifurcation depending on the value of scaled control gain followed by nu-

merical simulation results presented in section VI. Section VII concludes the paper.

2 Mathematical model

The focus of this paper is to investigate the dynamics of a n-unicycle system where the trajectory of the leader is characterized by constant linear and angular velocities (V and ω)

$$\begin{aligned} v_0 &= V, \\ \omega_0 &= \omega. \end{aligned} \quad (1)$$

The case $\omega = 0$ represents straight line motion, while $\omega \neq 0$ corresponds to circular motion. The position and orientation of the j^{th} vehicle ($j = 0$ for the leader and $j \geq 1$ for the follower) are denoted by $(x_j, y_j)^T \in \mathbb{R}^2$ and $\theta_j \in [-\pi, \pi)$, respectively. The kinematic equations for the follower are

$$\begin{pmatrix} \dot{x}_j(t) \\ \dot{y}_j(t) \\ \dot{\theta}_j(t) \end{pmatrix} = \begin{pmatrix} \cos \theta_j(t) & 0 \\ \sin \theta_j(t) & 0 \\ 0 & 1 \end{pmatrix} \begin{pmatrix} v_j \\ \omega_j \end{pmatrix}, \quad (2)$$

where $j \in \mathbb{Z}$, $j = 0, 1, \dots, n-1$, $(v_j, \omega_j)^T \in \mathbb{R}^2$ are control inputs (linear velocity and angular velocity).

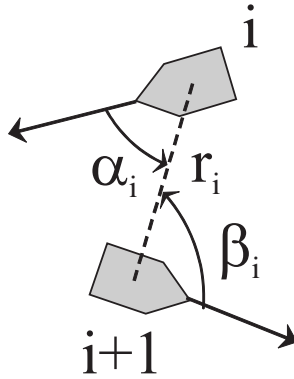


Figure 1: Relative coordinates with vehicle $i + 1$ pursuing vehicle i

The configuration of n-unicycle system is shown in Fig. 1, where r_i is the relative distance between the two vehicles, α_i is the angle between the current orientation of the i^{th} unicycle and the line of sight, and β_i is the angle between the current orientation of $i + 1^{\text{th}}$ unicycle and the line of sight. Both angles are positive in the sense of counterclockwise rotation to the line of sight. Following

[14], the kinematic equations are written in relative coordinates:

$$\begin{cases} \dot{r}_0 = -v_0 \cos \alpha_0 - v_1 \cos \beta_0, \\ \dot{\alpha}_0 = \frac{1}{r_0}(v_0 \sin \alpha_0 + v_1 \sin \beta_0) - \omega_0, \\ \dot{\beta}_0 = \frac{1}{r_0}(v_0 \sin \alpha_0 + v_1 \sin \beta_0) - \omega_1, \\ \dot{r}_i = -v_i \cos \alpha_i - v_{i+1} \cos \beta_i, \\ \dot{\alpha}_i = \frac{1}{r_i}(v_i \sin \alpha_i + v_{i+1} \sin \beta_i) - \omega_i, \\ \dot{\beta}_i = \frac{1}{r_i}(v_i \sin \alpha_i + v_{i+1} \sin \beta_i) - \omega_{i+1}, \end{cases} \quad (3)$$

where $i \in \mathbb{Z}$, $i = 1, \dots, n-2$, $r_i \in \mathbb{R}^+$ and $(\alpha_i, \beta_i) \in \mathcal{S}^1 \times \mathcal{S}^1$. The pursuit control law for the i^{th} follower is chosen as

$$\begin{aligned} v_i &= r_{i-1}, \\ \omega_i &= k \sin \beta_{i-1}, \end{aligned} \quad (4)$$

where the gain k is positive. The choice of this control law is inspired by the goal to align the follower's instantaneous velocity vector with its line of sight.

Substituting the control laws (1) and (4) into the relative dynamics (3) yields $n-1$ sets of 3-D ODEs:

$$\begin{cases} \dot{r}_0 = -V \cos \alpha_0 - r_0 \cos \beta_0, \\ \dot{\alpha}_0 = \frac{1}{r_0}(V \sin \alpha_0 + r_0 \sin \beta_0) - \omega, \\ \dot{\beta}_0 = \frac{1}{r_0}(V \sin \alpha_0 + r_0 \sin \beta_0) - k \sin \beta_0, \\ \dot{r}_i = -r_{i-1} \cos \alpha_i - r_i \cos \beta_i, \\ \dot{\alpha}_i = \frac{1}{r_i}(r_{i-1} \sin \alpha_i + r_i \sin \beta_i) - k \sin \beta_{i-1}, \\ \dot{\beta}_i = \frac{1}{r_i}(r_{i-1} \sin \alpha_i + r_i \sin \beta_i) - k \sin \beta_i, \end{cases} \quad (5)$$

The parameters of this system are V , ω and k and are restricted to be positive.

3 Characterization of equilibria

3.1 Derivation of the fixed points

Setting the right hand side of (5) to zero results $3n-3$ transcendental equations for the fixed points of the system

$$\frac{V}{r_0^*} \cos \alpha_0^* = -\cos \beta_0^*, \quad (6)$$

$$\frac{V}{r_0^*} \sin \alpha_0^* = -\sin \beta_0^* + \omega, \quad (7)$$

$$\frac{V}{r_0^*} \sin \alpha_0^* = (k-1) \sin \beta_0^*, \quad (8)$$

$$\frac{r_{i-1}^*}{r_i^*} \cos \alpha_i^* = -\cos \beta_i^*, \quad (9)$$

$$\frac{r_{i-1}^*}{r_i^*} \sin \alpha_i^* = -\sin \beta_i^* + k \sin \beta_{i-1}^*, \quad (10)$$

$$\frac{r_{i-1}^*}{r_i^*} \sin \alpha_i^* = (k-1) \sin \beta_i^*. \quad (11)$$

Subtracting (7) from (8) and (10) from (11) yields

$$\sin \beta_0^* = \sin \beta_1^* = \cdots = \sin \beta_{n-2}^* = \frac{\omega}{k}. \quad (12)$$

Fixed point(s) exist when $|\sin \beta^*| \leq 1$, i.e. $k \geq \omega$. When $k = \omega$, fixed points coalesce in a saddle-node bifurcation.

Squaring and adding (6) and (7), (9) and (10) yields

$$\left(\frac{V}{r_0^*}\right)^2 = \left(\frac{r_{i-1}^*}{r_i^*}\right)^2 = 1 + \omega^2 - \frac{2\omega^2}{k},$$

which results the equilibrium relative distance as

$$r_0^* = \frac{V}{\sqrt{1 + \omega^2 - \frac{2\omega^2}{k}}},$$

$$r_i^* = \frac{V}{\left(1 + \omega^2 - \frac{2\omega^2}{k}\right)^{\frac{i+1}{2}}}, \quad 1 + \omega^2 - \frac{2\omega^2}{k} > 0, \quad i = 1, 2, \dots, n-2. \quad (13)$$

Further, substituting (12) and (13) into (7) and (10) yields

$$\sin \alpha_0^* = \sin \alpha_1^* = \cdots = \sin \alpha_{n-2}^* = \frac{\omega - \frac{\omega}{k}}{\sqrt{1 + \omega^2 - \frac{2\omega^2}{k}}}. \quad (14)$$

From (6) and (9), it can be noted that $\cos \alpha_i^*$ and $\cos \beta_i^*$ must have different signs.

When $k > \omega$, every α_i^* can assume two distinct values in $[0, 2\pi]$ and thus there are 2^{n-1} possible fixed points of system (5). However $2^{n-1} - 2$ of these fixed points are spurious, as the geometric constraint of the equilibrium formation demands all unicycles to perform unidirectional translation in case of straight line formation and unidirectional rotation in case of cyclic formation. This constraint makes only the following two fixed points (*A* and *B*) possible:

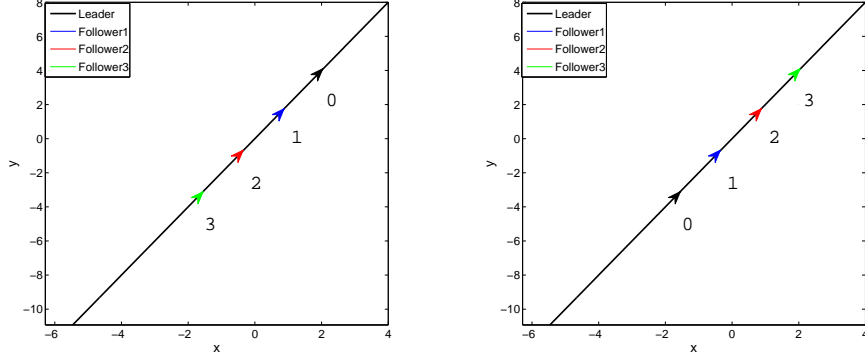
$$A \left\{ \begin{array}{l} r_0^* = \frac{V}{\sqrt{1 + \omega^2 - \frac{2\omega^2}{k}}}, \quad r_i^* = \frac{V}{\left(1 + \omega^2 - \frac{2\omega^2}{k}\right)^{\frac{i+1}{2}}}, \\ \alpha_0^* = \alpha_1^* = \cdots = \alpha_{n-2}^* = \pi - \arcsin \omega \frac{k-1}{k\sqrt{1 + \omega^2 - \frac{2\omega^2}{k}}}, \\ \beta_0^* = \beta_1^* = \cdots = \beta_{n-2}^* = \arcsin \frac{\omega}{k}, \end{array} \right.$$

$$B \left\{ \begin{array}{l} r_0^* = \frac{V}{\sqrt{1 + \omega^2 - \frac{2\omega^2}{k}}}, \quad r_i^* = \frac{V}{\left(1 + \omega^2 - \frac{2\omega^2}{k}\right)^{\frac{i+1}{2}}}, \\ \alpha_0^* = \alpha_1^* = \cdots = \alpha_{n-2}^* = \arcsin \omega \frac{k-1}{k\sqrt{1 + \omega^2 - \frac{2\omega^2}{k}}}, \\ \beta_0^* = \beta_1^* = \cdots = \beta_{n-2}^* = \pi - \arcsin \frac{\omega}{k}, \end{array} \right.$$

When $k = \omega$, the two fixed points *A* and *B* coalesce in a saddle-node bifurcation.

3.2 Equilibrium formations

Fixed points *A* and *B* correspond to equilibrium formations in global coordinates (x, y, θ) . The goal of this section is to characterize these formations, as these



(a) Equilibrium formation for fixed point A (b) Equilibrium formation for fixed point B

Figure 2: Corresponding straight-line motion in global coordinates for fixed points A and B

correspond to the physical behavior of the leader-follower system. When $\omega = 0$, the trajectory of the leader can be expressed explicitly as

$$\begin{aligned} x_0(t) &= (V \cos \theta_0)t + x_0(0), \\ y_0(t) &= (V \sin \theta_0)t + y_0(0), \\ \theta_0(t) &= \theta_0(0), \end{aligned} \quad (15)$$

where $(x_0(0), y_0(0), \theta_0(0))$ are its initial positions and orientation. It is straightforward to observe that fixed points $A = (r_i^*, \alpha_i^*, \beta_i^*) = (V, \pi, 0)$ and $B = (r_i^*, \alpha_i^*, \beta_i^*) = (V, 0, \pi)$ correspond to rectilinear motion of the followers. Fig. 2 shows the corresponding “pursuit graph” (parametric plots of $\{x_i(t), y_i(t)\}$) of fixed A and fixed point B for this rectilinear motion. It can be noted that for fixed point A , the leader “leads the pack” and for fixed point B , it “trails the pack”.

When $\omega \neq 0$, the trajectory of the leader becomes

$$\begin{aligned} x_0(t) &= \frac{V}{\omega} \sin(\omega t + \theta) + x_c, \\ y_0(t) &= -\frac{V}{\omega} \cos(\omega t + \theta) + y_c, \end{aligned} \quad (16)$$

$$\theta_0(t) = \omega t + \theta_0(0), \quad (17)$$

where $x_c = x_0(0) - \frac{V}{\omega} \sin \theta_0(0)$ and $y_c = y_0(0) + \frac{V}{\omega} \cos \theta_0(0)$ are the center of the circle of radius $R_0 = \frac{V}{\omega}$ traversed by the leader. Without loss of generality we choose $x_c = y_c = 0$.

Both fixed points A and B yield the following two equations for the locus of the i^{th} follower

$$r_i^{*2} = \frac{V^2}{(1 + \omega^2 - \frac{2\omega^2}{k})^i} = x_i^2 + y_i^2 + x_{i+1}^2 + y_{i+1}^2 - 2(x_i x_{i+1} + y_i y_{i+1}), \quad (18)$$

$$\begin{aligned}\sin \alpha_i^* &= \frac{\omega - \frac{\omega}{k}}{\sqrt{1 + \omega^2 - \frac{2\omega^2}{k}}} = \sin \arctan \left(\frac{y_{i+1} - y_i}{x_{i+1} - x_i} - \theta_i \right) \\ &= \frac{x_i^2 + y_i^2 - x_i x_{i+1} - y_i y_{i+1}}{r_i^* \sqrt{x_{i+1}^2 + y_{i+1}^2}}.\end{aligned}\quad (19)$$

Since $x_0^2 + y_0^2 = \frac{V^2}{\omega^2}$ corresponds to the leader's ($j = 0$) trajectory, combining (18) and (19) results

$$x_1^2 + y_1^2 = \frac{V^2}{\omega^2} \frac{1}{1 + \omega^2 - \frac{2\omega^2}{k}} = R_1^2. \quad (20)$$

In general, using method of induction

$$x_j^2 + y_j^2 = \frac{V^2}{\omega^2} \frac{1}{(1 + \omega^2 - \frac{2\omega^2}{k})^j} = R_j^2. \quad (21)$$

This means that in the equilibrium formation, the j^{th} follower is circling the origin with radius R_j . Fig. 3 shows the corresponding ‘‘pursuit graph’’ for fixed A and fixed point B for circular motion ($\omega > 0$).

It can be noted from (21) that depending on the value of k , the concentric circles traced out by the followers can be inside ($k > 2$), on ($k = 2$) or outside ($k < 2$) the leader's circle. Also, analogous to Fig. 2, for $k > 2$ case, corresponding to fixed point A , the leader ‘‘leads the pack’’ i.e. the followers have positive phase difference with respect to the leader (Fig. 3a). Similarly, for fixed point B , the leader ‘‘trails the pack’’ i.e. the followers have negative phase difference with respect to the leader (Fig. 3b).

As discussed in the previous section, when $k = \omega > 1$, the two fixed points A and B coalesce to give rise to the single fixed point $(r_i^*, \alpha_i^*, \beta_i^*) = (\frac{V}{(\omega-1)^{i+1}}, \frac{\pi}{2}, \frac{\pi}{2})$ (Fig. 4a). When $k = \omega < 1$, the single fixed point becomes $(r_i^*, \alpha_i^*, \beta_i^*) = (\frac{V}{(1-\omega)^{i+1}}, -\frac{\pi}{2}, \frac{\pi}{2})$ (Fig. 4b).

4 Local stability analysis

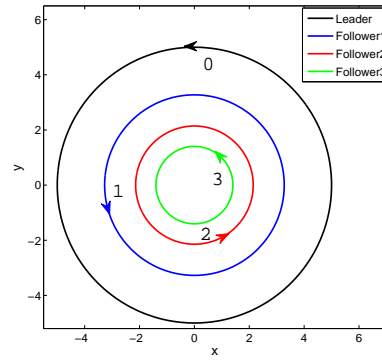
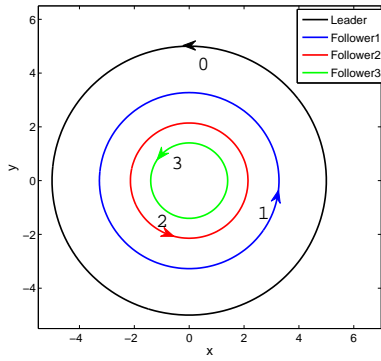
4.1 Linearization about the fixed points

The local stability of the fixed points is determined by the eigenstructure of the Jacobian evaluated at the fixed point. The Jacobian of (5) is given by:

$$\mathcal{J}_p = \begin{pmatrix} \mathbf{A}_0 & \mathbf{0} & \cdots & \mathbf{0} \\ \mathbf{B}_1 & \mathbf{A}_1 & \cdots & \mathbf{0} \\ \vdots & \ddots & \ddots & \vdots \\ \mathbf{0} & \cdots & \mathbf{B}_{n-2} & \mathbf{A}_{n-2} \end{pmatrix}, \quad (22)$$

where \mathbf{A}_i , \mathbf{B}_i and $\mathbf{0}$ are all 3×3 matrices.

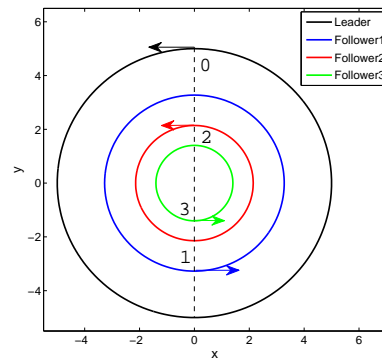
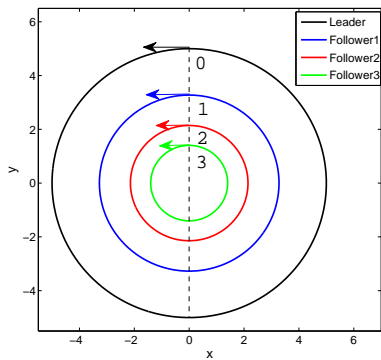
$$\mathbf{A}_0 = \begin{pmatrix} -\cos \beta_0^* & V \sin \alpha_0^* & r_0^* \sin \beta_0^* \\ -\frac{V}{r_0^{*2}} \sin \alpha_0^* & \frac{V}{r_0^*} \cos \alpha_0^* & \cos \beta_0^* \\ -\frac{V}{r_0^{*2}} \sin \alpha_0^* & \frac{V}{r_0^*} \cos \alpha_0^* & (1-k) \cos \beta_0^* \end{pmatrix},$$



(a) Equilibrium formation for fixed point A

(b) Equilibrium formation for fixed point B

Figure 3: Corresponding circular motion in global coordinates for fixed points A and B



(a) Equilibrium formation when $k = \omega > 1$

(b) Equilibrium formation when $k = \omega < 1$

Figure 4: Corresponding circular motion in global coordinates for the coalesced fixed point

$$\mathbf{A}_i = \begin{pmatrix} -\cos \beta_i^* & r_{i-1}^* \sin \alpha_i^* & r_i^* \sin \beta_i^* \\ -\frac{r_{i-1}^*}{r_i^*} \sin \alpha_i^* & \frac{r_{i-1}^*}{r_i^*} \cos \alpha_i^* & \cos \beta_i^* \\ -\frac{r_{i-1}^*}{r_i^*} \sin \alpha_i^* & \frac{r_{i-1}^*}{r_i^*} \cos \alpha_i^* & (1-k) \cos \beta_i^* \end{pmatrix}, \quad i = 1, 2, \dots, n-2,$$

$$\mathbf{B}_i = \begin{pmatrix} -\cos \alpha_i^* & 0 & 0 \\ \frac{\sin \alpha_i^*}{r_i^*} & 0 & -k \cos \beta_{i-1}^* \\ \frac{\sin \alpha_i^*}{r_i^*} & 0 & 0 \end{pmatrix}, \quad i = 1, 2, \dots, n-2,$$

The eigenvalues of (22) are also the eigenvalues of all \mathbf{A}_i 's since the Jacobian (22) is lower triangular block matrix. The characteristic polynomial for any of the \mathbf{A}_i 's evaluated at the fixed points have the same form and are given by (+ and - corresponds to fixed point A and B , resp.):

$$\lambda^3 \pm p_2 \lambda^2 + p_1 \lambda \pm p_0 = 0, \quad (23)$$

where $p_2 = (1 + \frac{1}{k})\sqrt{k^2 - \omega^2}$, $p_1 = \omega^2 + 2k - \frac{3\omega^2}{k}$ and $p_0 = (1 + \omega^2 - \frac{2\omega^2}{k})\sqrt{k^2 - \omega^2}$. The characteristic equation corresponding to fixed point B can be obtained from that of fixed point A by the transformation $\lambda \rightarrow -\lambda$, so the spectrum of B is the reflection of that of A about the imaginary axis.

4.2 Linear stability boundary

A fixed point is stable when the corresponding characteristic polynomial is Hurwitz. Necessary and sufficient condition on Hurwitz stability of a third order polynomial is given on page 132 of [32], requiring $p_0, p_1, p_2 > 0$ and $p_1 p_2 > p_0$ for (23), which results

$$2k^3 + k^2 - 3\omega^2 > 0, \quad (24)$$

$$1 + \omega^2 - \frac{2\omega^2}{k} > 0. \quad (25)$$

From (12), the existence of the fixed points requires

$$k \geq \omega. \quad (26)$$

Inequalities (24), (25) and (26) determine regions in the $k - \omega$ parameter space where fixed points exists, as well as their stability. These regions are characterized by the three curves $\omega_1(k) = k$, $\omega_2(k) = \sqrt{\frac{2k^3 + k^2}{3}}$ and $\omega_3(k) = \sqrt{\frac{k}{2-k}}$ ($k < 2$). Notice that when $k \geq 2$, inequality (25) is always satisfied, the stability region is determined only by the remaining two curves. It can be easily verified that $\omega_1(k) \leq \omega_3(k)$ when $0 < k < 2$. Fig. 5 depicts the stability boundaries of this system. It can be observed that when $\omega = 0$ (straight line motion), fixed point A is always a stable node while B is always an unstable one.

5 Andronov-Hopf bifurcation

When $0 < k < 1$, the characteristic polynomial on the curve $\omega_2(k)$ can be written as

$$(\lambda + (1 + \frac{1}{k})\sqrt{k^2 - \omega^2})(\lambda^2 + \omega^2 + 2k - \frac{3\omega^2}{k}) = 0.$$

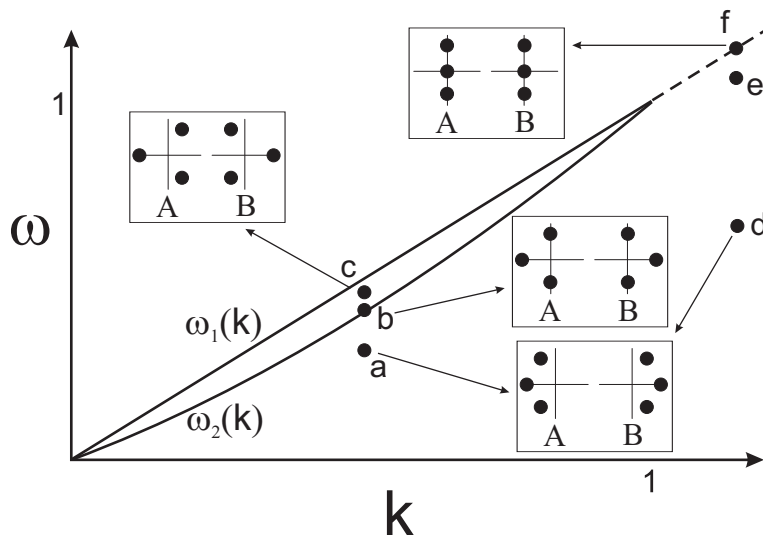


Figure 5: Linear stability boundary for system (5) with spectra of A and B

This implies that for the fixed point A , the Jacobian has one negative real eigenvalue and a complex conjugate pair on the imaginary axis. Below the curve $\omega_2(k)$, the Jacobian has one negative real eigenvalue and a pair of complex conjugates on the left half plane, i.e. the fixed point is a stable node-focus. Between the curve $\omega_2(k)$ and $\omega_1(k)$, the pair of complex conjugate eigenvalues have positive real part, which suggests the occurrence of Andronov-Hopf bifurcation by increasing k through $\omega_2(k)$. On this curve, the critical bifurcation value of ω is $\omega_c = \sqrt{\frac{2k^3+k^2}{3}}$, and the root crossing velocity can be calculated as

$$\operatorname{Re} \frac{d\lambda}{d\omega} \Big|_{(k, \omega_c)} = \frac{3\sqrt{2}}{7k+2} \sqrt{\frac{1+2k}{1-k}} > 0. \quad (27)$$

Transversal root crossing is a necessary condition for the Andronov-Hopf bifurcation. It can be noted that for the case of n unicycles, we have $n-1$ identical triplets of such eigenvalues. This implies that the system undergoes Andronov-Hopf bifurcation when $n=2$, double-Hopf bifurcation when $n=3$ and in general, a bifurcation with $(n-1)$ pairs of pure imaginary eigenvalues. The rest of this section analyzes the two unicycle case in detail.

To show that the fixed point of the dynamical system (5) is weakly attracting/repelling on the stability boundary, one needs to compute the so-called Poincaré-Lyapunov constant [33]. To find this constant, the original equation (5) is expanded up to third order around fixed point A [34]

$$\dot{\mathbf{w}} = \Psi(\mathbf{w}) = \mathcal{J}_p \mathbf{w} + \frac{1}{2} \mathbf{f}^{(2)}(\mathbf{w}) + \frac{1}{6} \mathbf{f}^{(3)}(\mathbf{w}) + \mathcal{O}(\mathbf{w}^4), \quad (28)$$

where $\mathbf{w} = (r - r_A^*, \alpha - \alpha_A^*, \beta - \beta_A^*)^T$ defines new coordinates which shift the fixed point A to the origin. In these new coordinates, $\mathbf{f}^{(2)}(\mathbf{w})$ and $\mathbf{f}^{(3)}(\mathbf{w})$ are multilinear vector functions given by

$$\mathbf{f}_i^{(2)} = \sum_{j,k=1}^n \frac{\partial^2 \Psi_i(\xi)}{\partial \xi_j \partial \xi_k} \Big|_{\xi=0} \mathbf{w}_j \mathbf{w}_k \quad i = 1, 2, 3,$$

and

$$\mathbf{f}_i^{(3)} = \sum_{j,k,l=1}^n \frac{\partial^3 \Psi_i(\xi)}{\partial \xi_j \partial \xi_k \partial \xi_l} \Big|_{\xi=0} \mathbf{w}_j \mathbf{w}_k \mathbf{w}_l \quad i = 1, 2, 3.$$

In order to obtain the real Jordan canonical form, a linear transformation \mathbf{T} needs to be constructed using the eigenvectors of the Jacobian evaluated at ω_c . At the critical point, the pair of complex conjugate eigenvalues have the form $\lambda_{2,3} = \pm i\omega_0$,

$$\omega_0 = \sqrt{k(1 - \frac{2}{3}k)(1 - k)} > 0.$$

Let $\mathbf{q}_2 \in \mathcal{C}^3$ be the complex eigenvector corresponding to the eigenvalue λ_2 . Then,

$$\mathcal{J}_p \mathbf{q}_2 = i\omega_0 \mathbf{q}_2, \quad \mathcal{J}_p \bar{\mathbf{q}}_2 = -i\omega_0 \bar{\mathbf{q}}_2$$

Also, let $\mathbf{q}_1 \in \mathcal{R}^3$ be the real eigenvector corresponding to the eigenvalue $\lambda_1 = -(1+k)\sqrt{\frac{2}{3}(1-k)}$, i.e. $\mathcal{J}_p \mathbf{q}_1 = \lambda_1 \mathbf{q}_1$. The transformation matrix \mathbf{T} is composed by $\frac{1}{\|\mathbf{q}_1\|}(\text{Re}\mathbf{q}_2, -\text{Im}\mathbf{q}_2, \|\mathbf{q}_1\|\mathbf{q}_1)$ where \mathbf{q}_1 and \mathbf{q}_2 are given by

$$\mathbf{q}_2 = \begin{pmatrix} \frac{2\sqrt{6}Vk}{9\gamma\sqrt{1-k}} + i\frac{Vk(1-\frac{2}{3}k)}{3\omega_0\gamma} \\ 1 \\ 1 - \frac{2}{3}k + i\frac{\sqrt{6}\omega_0}{3\sqrt{1-k}} \end{pmatrix}, \quad \mathbf{q}_1 = \begin{pmatrix} -\frac{\sqrt{6}V(1+2k)}{3\gamma\sqrt{1-k}} \\ 1 \\ k+1 \end{pmatrix}$$

$$\gamma = \frac{1}{3}\sqrt{(3-2k)(1+2k)(1-k^2)}.$$

Introducing the transformation $\mathbf{y} = \mathbf{T}^{-1}\mathbf{w}$

$$\dot{\mathbf{y}} = \mathbf{J}\mathbf{y} + \frac{1}{2}\mathbf{g}^{(2)}(\mathbf{y}) + \frac{1}{6}\mathbf{g}^{(3)}(\mathbf{y}) + \mathcal{O}(\mathbf{y}^4), \quad (29)$$

where the Jordan canonical form \mathbf{J} is given by

$$\mathbf{J} = \mathbf{T}^{-1}\mathcal{J}_p\mathbf{T} = \begin{pmatrix} 0 & -\omega_0 & 0 \\ \omega_0 & 0 & 0 \\ 0 & 0 & \lambda_1 \end{pmatrix}.$$

In (29), the nonlinear vector functions in transformed coordinates are given by

$$\mathbf{g}^{(2)}(\mathbf{y}) = \mathbf{T}^{-1}\mathbf{f}^{(2)}(\mathbf{w})|_{\mathbf{w}=\mathbf{T}\mathbf{y}},$$

$$\mathbf{g}^{(3)}(\mathbf{y}) = \mathbf{T}^{-1}\mathbf{f}^{(3)}(\mathbf{w})|_{\mathbf{w}=\mathbf{T}\mathbf{y}}.$$

Assuming that the center manifold has the quadratic form $y_3 = \frac{1}{2}(h_1 y_1^2 + 2h_2 y_1 y_2 + h_3 y_2^2)$, one can reduce (29) into a two-dimensional system up to third

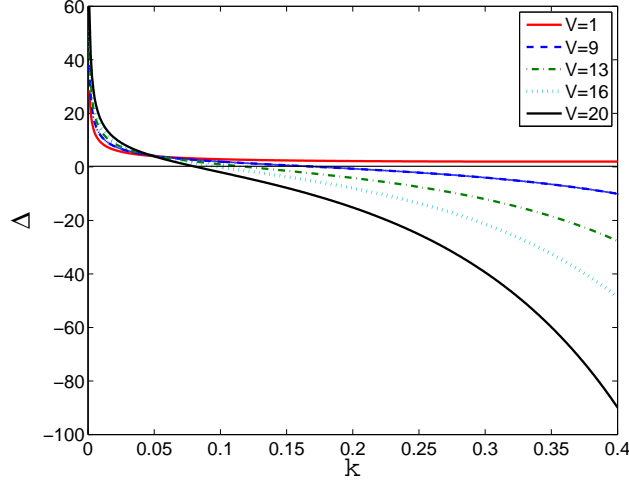


Figure 6: Variation of Poincaré-Lyapunov constant (Δ) with control gain (k)

order

$$\begin{aligned}
\dot{y}_1 &= -\omega_0 y_2 + a_{20} y_1^2 + a_{11} y_1 y_2 + a_{02} y_2^2 \\
&\quad + a_{30} y_1^3 + a_{21} y_1^2 y_2 + a_{12} y_1 y_2^2 + a_{03} y_2^3, \\
\dot{y}_2 &= \omega_0 y_1 + b_{20} y_1^2 + b_{11} y_1 y_2 + b_{02} y_2^2 \\
&\quad + b_{30} y_1^3 + b_{21} y_1^2 y_2 + b_{12} y_1 y_2^2 + b_{03} y_2^3.
\end{aligned} \tag{30}$$

Using the 10 out of these 14 coefficients a_{jk}, b_{jk} , the so called Poincaré-Lyapunov constant Δ can be calculated as [33]

$$\begin{aligned}
\Delta &= \frac{1}{8\omega} ((a_{20} + a_{02})(a_{11} - b_{20} + b_{02}) \\
&\quad + (b_{20} + b_{02})(a_{02} - a_{20} - b_{11})) \\
&\quad + \frac{1}{8}(3a_{30} + a_{12} + b_{21} + 3b_{03}).
\end{aligned} \tag{31}$$

Fig. 6 illustrates the variation of Δ with respect to k . Note that based on the value of parameter V , the Andronov-Hopf bifurcation can be supercritical ($\Delta > 0$) or subcritical ($\Delta < 0$).

6 Numerical Results

6.1 Andronov-Hopf bifurcation

Fig. 7 shows the phase portrait corresponding to point a ($k = 0.500, \omega = 0.301$) on the stability chart (Fig. 5) and the associated pursuit graph. Fixed point A is exponentially attracting here. Fig. 8 depicts the phase portrait associated with point b ($k = 0.500, \omega = 0.408$) showing a weakly attracting fixed point

A. There is a stable limit cycle born (supercritical Andronov-Hopf bifurcation) around the fixed point A (point c) when ω is increased through its critical value ω_c (phase portrait and pursuit graph are shown in Fig. 9). The pursuit trajectory in global coordinates has two harmonic components.

Fig. 10a shows the “pursuit graph” of five unicycles (initial conditions are chosen slightly away from the equilibrium formation) when ω lies slightly above the curve $\omega_2(k)$ (point c). It shows that the fourth follower exhibits most quasi-periodic behavior. The vigor of such quasi-periodicity decreases with the proximity to the leader. Fig. 10b corroborates this fact by showing that further the follower is, the wider its frequency spectrum becomes.

6.2 Fold-Hopf bifurcation

When $k > 1$, the characteristic polynomial on the stability curve $\omega_1(k)$ can be written as

$$\lambda^3 + (\omega^2 - \omega)\lambda = 0$$

implying that there is zero eigenvalue together with a pair of pure imaginary ones. This is a Fold-Hopf (a codimension-two) bifurcation [33]. Fig. 11.a and Fig. 11.c show the phase portrait of point f ($k = 1.20, \omega = 1.20$) on the stability curve $k = \omega$ and the corresponding pursuit graph, while Fig. 11.b shows the phase portrait of point e situated slightly below the point f .

For the case of five unicycles (initial conditions are chosen slightly away from the equilibrium formation), the time series and the corresponding FFT for the followers are plotted in Fig. 12. It shows that the third and fourth follower exhibit complex behavior with possibly heteroclinic bursts between quasi-periodic and chaotic behavior.

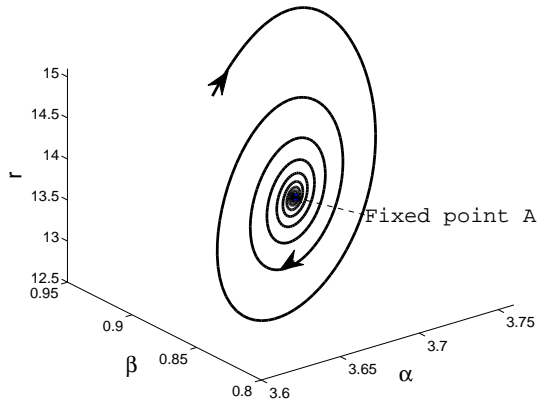
6.3 Global Bifurcations

In addition to the Andronov-Hopf and Fold-Hopf bifurcations, preliminary simulations indicate global bifurcations involving the destruction of heteroclinic orbits. Fig. 13 shows the phase portrait corresponding to point d ($k = 1.20, \omega = 0.60$), with a heteroclinic orbit (trajectory 1) connecting fixed points A and B . When k is decreased below 1, it was observed that the heteroclinic orbit disappear and the region of attraction for fixed point A shrinks significantly.

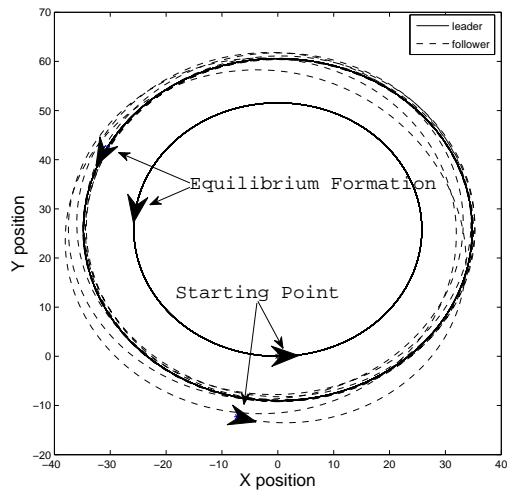
The dynamics is very interesting when k is around 1 (the intersection of the saddle-node and Andronov-Hopf bifurcation curves). When $(k, \omega) = (1.01, 1)$, one can observe a heteroclinic orbit or periodic motions containing higher harmonics as shown in Fig. 14.

7 Conclusions

In this paper, the leader-follower pursuit of unicycles is studied. Local stability analysis around the equilibrium formation has been performed. Analysis and numerical simulations have shown the existence of Andronov-Hopf and Fold-Hopf bifurcations on the stability boundary. In addition to the results provided here, the authors have also studied the effect of constant communication delay between the unicycles in leader-follower configuration. Both analytical and numerical results (not provided here) show that for a suitable distributed control



(a) Phase portrait at point a



(b) Pursuit graph for point a in global coordinates

Figure 7: Phase portrait at point a when fixed point A is attracting and the corresponding pursuit graph in global coordinates

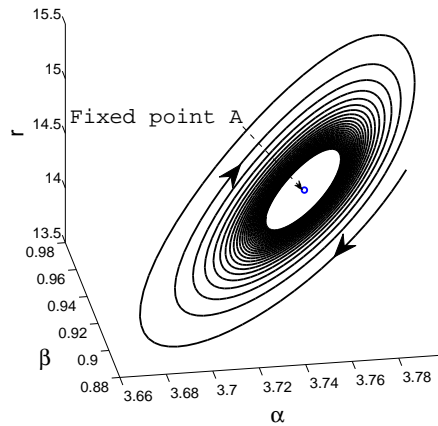
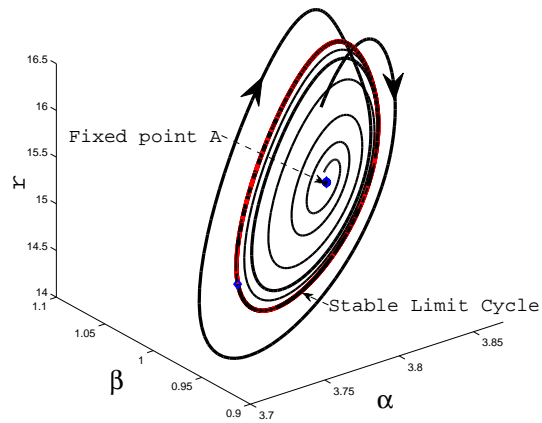


Figure 8: Phase portrait at point b where the fixed point A is a weakly attracting one

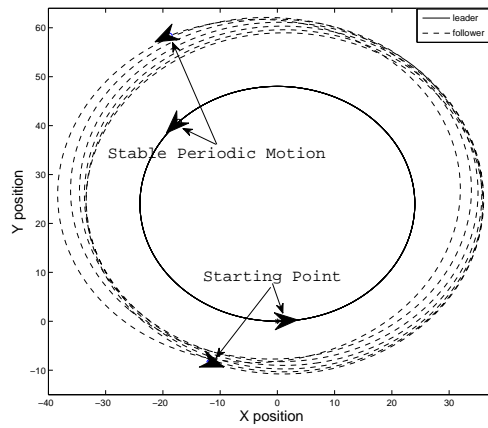
law, where one may ignore the transients of the agent response, the communication has no qualitative effect on the final consensus dynamics of the agent collective. As briefly stated in Section I, the future research direction includes the more generalized nonlinear dynamic analysis of two unicycles, not necessarily in leader-follower configuration and extending the result for multiple unicycles with communication delay.

References

- [1] J. K. Parrish, S. V. Viscido, and D. Grünbaum, Self-organized Fish Schools: An Examination of Emergent Properties. *Biol. Bull.*, 202: 296-305, 2002.
- [2] H.-S., Niwa, Newtonian Dynamical Approach to Fish Schooling. *Journal of Theoretical Biology*, 181: 47-63, 1996.
- [3] S. Gueron, S. A. Levin, and D. I. Rubenstein, The Dynamics of Herds: From Individuals to Aggregations. *Journal of Theoretical Biology*, 182: 85-98, 1996.
- [4] C. W. Reynolds, Flocks, Herds and Schools: A Distributed Behavioral Model. *Computer Graphics*, 21 (4): 25-34, 1987.
- [5] C. R. McInnes, Distributed Control for On-orbit Assembly. *Advances in the Astronautical Sciences*, 90: 2079-2092, 1996.
- [6] E. Justh, and P. Krishnaprasad, A Simple Control Law for UAV Formation Flying. Technical Report, TR 2002-38, Institute for Systems Research, University of Maryland, 2002.
- [7] Y. Cao, W. Ren, N. Sorensen, L. Ballard, A. Reiter, and J. Kennedy, Experiments in Consensus-based Distributed Cooperative Control of Mul-

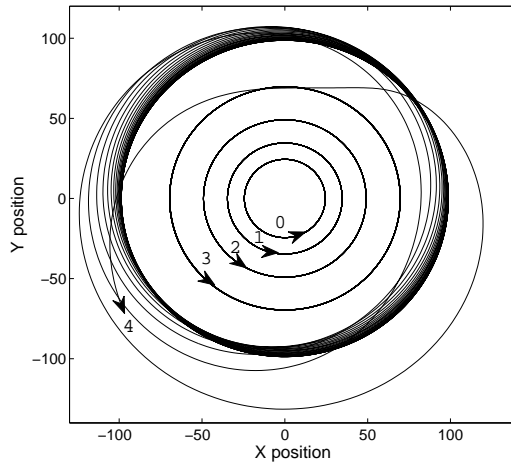


(a) Phase portrait at point c

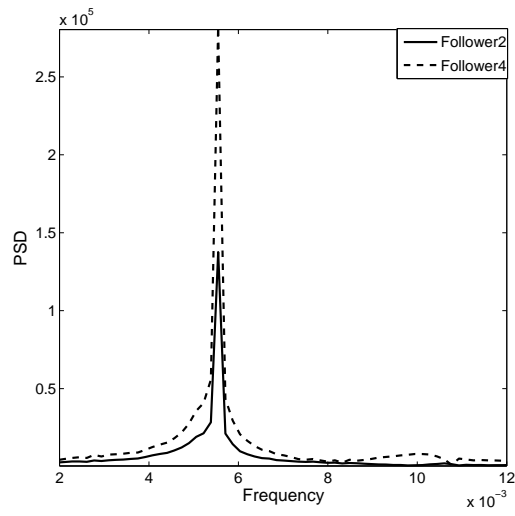


(b) Pursuit graph in global coordinates

Figure 9: Phase portrait at point c ($k = 0.500, \omega = 0.409$) when a stable limit cycle is born near fixed point A and the corresponding pursuit graph

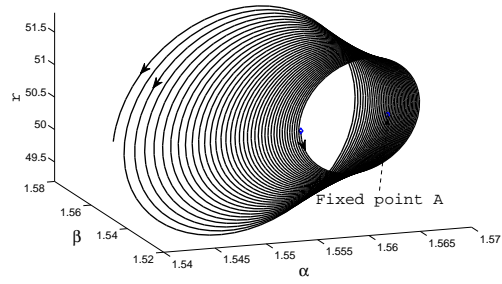


(a) Pursuit graph for five unicycles

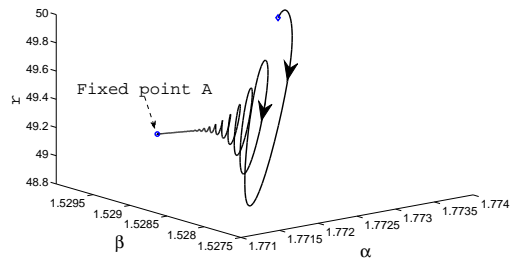


(b) Corresponding FFT of x_2 and x_4

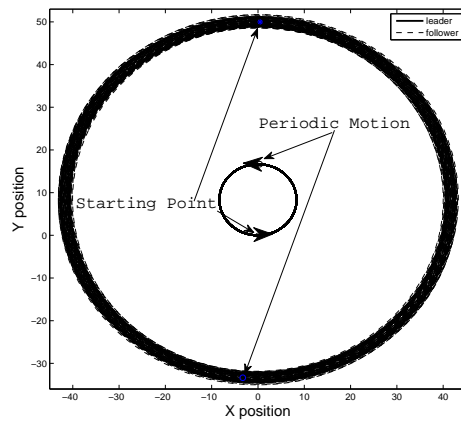
Figure 10: Pursuit graph and the corresponding FFT for five unicycle case at point c



(a) Phase portrait at point f

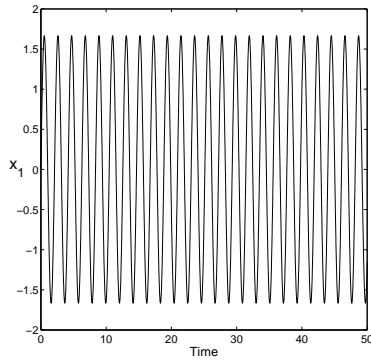


(b) Phase portrait at point e

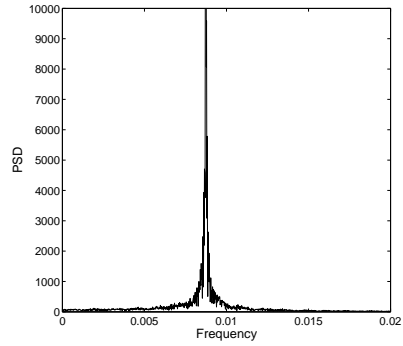


(c) Pursuit graph in global coordinates

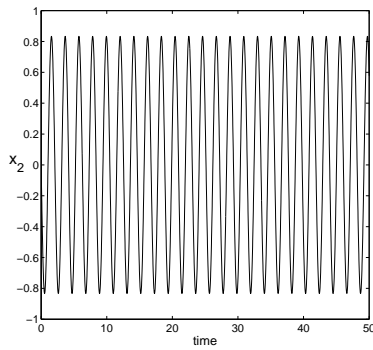
Figure 11: Phase portrait at point f near the fixed point A and the corresponding pursuit graph in global coordinates



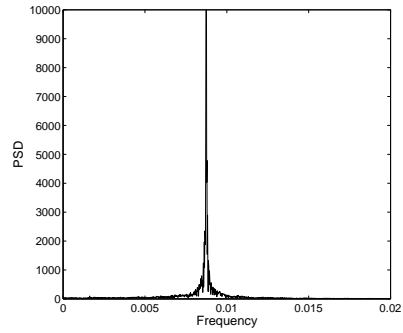
(a) Time series of X position of follower 1



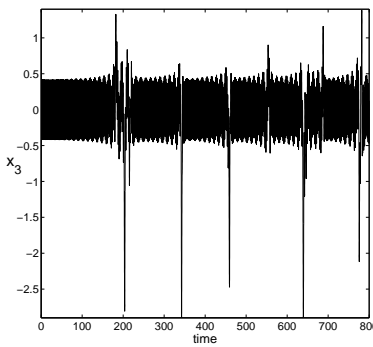
(b) FFT of follower 1



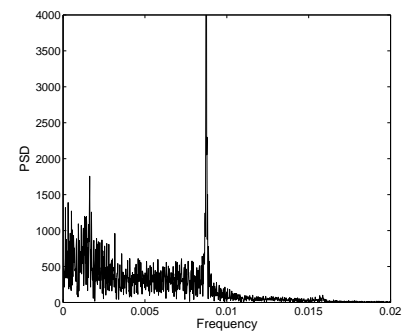
(c) Time series of X position of follower 2



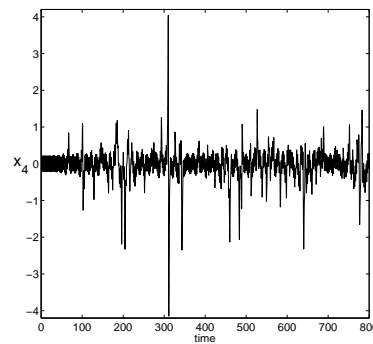
(d) FFT of follower 2



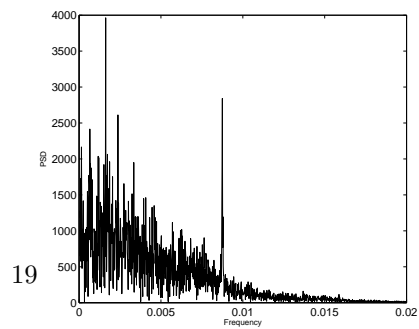
(e) Time series of X position of follower 3



(f) FFT of follower 3



(g) Time series of X position of follower 4



(h) FFT of follower 4

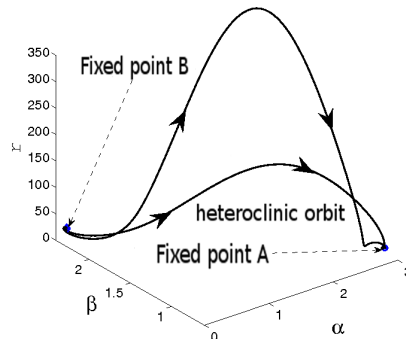
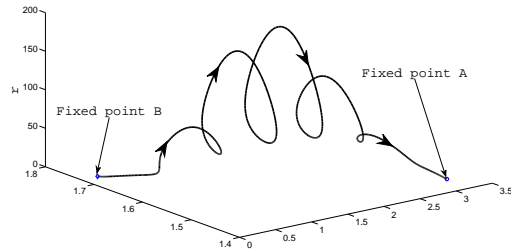


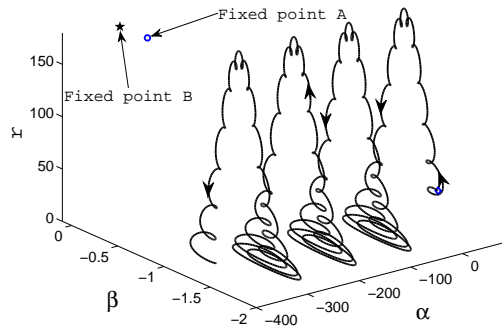
Figure 13: Heteroclinic orbit in the phase portrait at point d

tiple Mobile Robots. *Proc. of the 2007 IEEE International Conference on Mechatronics and Automation*, 2819-2824, 2007.

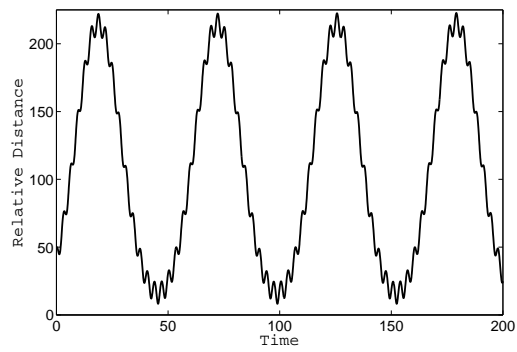
- [8] D. Helbing, I. Farkas, and T. Vicsek, Simulating Dynamical Features of Escape Panic. *Nature*, 407: 487-490, 2000.
- [9] L. Fang, and P. J. Antsaklis, On Communication Requirements for Multi-agent Consensus Seeking. *LNCS*, 331: 53-67, 2006.
- [10] D. V. Dimarogonas, and K. J. Kyriakopoulos, On the State Agreement Problem for Unicycles. *Proc. of the 2006 American Control Conference*, 2016-2021, 2006.
- [11] J. Lin, A. S. Morse, and B. D. O. Anderson, The Multi-agent Rendezvous Problem. *Proc. of the 42nd 2003 IEEE Conference on Decision and Control*, 1508-1513, 2003.
- [12] R. Olfati-Saber, and R. M. Murray, Consensus Problems in Networks of Agents with Switching Topology and Time-delays. *IEEE Transactions on Automatic Control*, 49 (9): 1520-1533, 2004.
- [13] A. Bernhart, Polygons of Pursuit. *Scripta Mathematica*, 24: 23-50, 1959.
- [14] J. A. Marshall, M. E. Broucke, and B. A. Francis, Formations of Vehicles in Cyclic Pursuit. *IEEE Transactions on Automatic Control*, 49 (11): 1963-1974, 2004.
- [15] J. A. Marshall, M. E. Broucke, and B. A. Francis, Pursuit Formations of Unicycles. *Automatica*, 42 (1): 3-12, 2006.
- [16] E. Justh, and P. Krishnaprasad, Steering laws and continuum models for planar formations. *Proc. of the 42nd 2003 IEEE Conference on Decision and Control*, 3609-3614, 2003.



(a) Heteroclinic orbit in the phase portrait when $(k, \omega) = (1.01, 1)$



(b) Periodic orbit in the phase portrait when $(k, \omega) = (1.01, 1)$



(c) Time series of the relative distance corresponding to the periodic orbit

Figure 14: System dynamics when $(k, \omega) = (1.01, 1)$

- [17] R. Sepulchre, D. Payley, and N. E. Leonard, Collective motion and oscillator synchronization. *Proc. of the 2003 Block Island Workshop on Cooperative Control*, V. Kumar, N. Leonard, and A. Morse, Eds. Springer Verlag, 189-205, 2005.
- [18] D. J. Klein, and K. A. Morgansen, Controlled collective motion for trajectory tracking. *2006 American Control Conference*, Minneapolis, Minnesota, June 2006.
- [19] J. P. Desai, J. P. Ostrowski, and V. Kumar, Modeling and Control of Formations of Nonholonomic Mobile Robots. *IEEE Transactions on Robotics and Automation*, 17 (6): 905-908, 2001.
- [20] A. K. Das, R. Fierro, V. Kumar, J. P. Ostrowski, J. Spletzer, and C. J. Taylor, A Vision-based Formation Control Framework. *IEEE Transactions on Robotics and Automation*, 18 (5): 813-825, 2002.
- [21] A. Jadbabaie, J. Lin, and A. S. Morse, Coordination of Groups of Mobile Autonomous Agents using Nearest Neighbor Rules. *IEEE Transactions on Automatic Control*, 48 (6): 988-1001, 2003.
- [22] P. Yang, R. A. Freeman, and K. M. Lynch, Multi-agent Coordination by Decentralized Estimation and Control, To appear, *IEEE Transactions on Automatic Control*, 2008.
- [23] R. A. Freeman, P. Yang, and K. M. Lynch, Distributed Estimation and Control of Swarm Formation Statistics. *2006 American Control Conference*, Minneapolis, Minnesota, 749-755, June 2006.
- [24] J. Lin, A. S. Morse, and B. D. O. Anderson, The Multi-agent Rendezvous Problem Part 2: The Asynchronous Case. *SIAM Journal on Control and Optimization*, 46 (6): 2120-2147, 2007.
- [25] L. Fang, P. J. Antsaklis, and A. Tzimas, Asynchronous Consensus Protocols: Preliminary Results, Simulations and Open Questions. *Proc. of the 44th 2005 IEEE Conference on Decision and Control*, 2194-2199, 2005.
- [26] Y. Liu, K. M. Passino, and M. Polycarpou, Stability Analysis of One-dimensional Asynchronous Swarms, *IEEE Transactions on Automatic Control*, 48(10): 1848-1854, 2003.
- [27] V. Gazi, Stability of an Asynchronous Swarm with Time-dependent Communication Links, *IEEE Transactions on Systems, Man and Cybernetics, Part B: Cybernetics*, 38(1): 267-274, 2008.
- [28] S. Zhao, and T. Kalmár-Nagy, Nonlinear Dynamics of Uni-cyclic Pursuit. *2008 IEEE Multi-Conference on Systems and Control*, 3-5 Sep. 2008, San Antonio, Texas, USA.
- [29] N. J. Mathai, and T. Zourntos, Emergent Fluctuations in the Trajectories of Agent Collectives. *Fluctuations and Noise Letters*, 7 (4): L429-L437, 2007.
- [30] D. Hammel, Formation Flight as an Energy Saving Mechanism. *Israel Journal of Zoology*, 41: 261-278, 1995.

- [31] M. Andersson, and J. Wallander, Kin Selection and Reciprocity in Flight Formation. *Behavioral Ecology*, 15 (1): 158-162, 2004.
- [32] W. S. Levine, Control System Fundamentals. *CRC Press*, 2000.
- [33] J. Guckenheimer, and P. Holmes, Nonlinear Oscillations, Dynamical Systems, and Bifurcations of Vector Fields. *Springer*, 1983.
- [34] Y.A. Kuznetsov, Elements of Applied Bifurcation Theory. *Springer*, 2004.